PHYSICAL REVIEW B **92**, 064401 (2015)

Schwinger boson mean field perspective on emergent spins in diluted Heisenberg antiferromagnets

Shivam Ghosh,[1] Hitesh J. Changlani,[2] and Christopher L. Henley[1,*]

[1]*Laboratory of Atomic And Solid State Physics, Cornell University, Ithaca, New York 14853, USA*

[2]*Department of Physics, University of Illinois at Urbana-Champaign, Urbana, Illinois 61801, USA*

(Received 1 June 2015; revised manuscript received 11 July 2015; published 3 August 2015)

Using an adaptation of Schwinger boson mean field theory (SBMFT) for nonuniform systems, we study the nature of low-energy spin excitations on the square and Bethe lattices at their percolation threshold. The optimal SBMFT parameters are interpreted as on-site potentials and pairing amplitudes, which enables an explanation of why emergent local moments develop in this system on dilution [L. Wang and A. W. Sandvik, Phys. Rev. Lett. **97**, 117204 (2006); H. J. Changlani *et al.*, *ibid.* **111**, 157201 (2013)] and why the corresponding single-particle frequencies are driven to *anomalously* low values. We discuss how our mean field calculations suggest the strong link between the presence of sublattice imbalance and long-range antiferromagnetic order and why linear spin wave theory is inadequate for capturing this relation. Within the SBMFT framework, we also extract an energy scale for the interaction between emergent moments, which show qualitative agreement with many-body calculations.

DOI: 10.1103/PhysRevB.92.064401 PACS number(s): 75.10.Jm, 75.40.Mg, 75.50.Ee, 75.10.Nr

I. INTRODUCTION

The concept of emergence is central to condensed-matter systems. This means that an effective low-energy description of a system can be made in terms of emergent degrees of freedom and interactions between them, which might have different properties compared to the original ingredients. For example, dilution of quantum magnets in the form of vacancies or substitution with nonmagnetic ions creates emergent local moments [1–5] which influence the spin texture [6], magnetic susceptibility [1,7], specific heat [1], and excitation spectra [4,5]. Recent work also shows how random on-site magnetic fields in spin chains create emergent composite spins which are exponentially localized in space, resulting in a nonequilibrated "many-body localized" state [8,9].

The subject of interest here is that of dilution to the percolation threshold, i.e., when the nonmagnetic impurities are randomly distributed and their number is macroscopically large enough to create a finitely ramified fractal cluster. In this case an anomalous energy scale in the low-energy spectrum appears, lower than the usual rotor states [10]. The presence of local regions with an excess of one kind of sublattice sites over another give rise to "dangling spins" [5], whose mutual interactions create low-energy quasidegenerate states [4]. The energy splittings are exponentially small in the average separation between two such emergent spins.

While many facets of this problem are now understood, a simple explanation for the decoupling of such a localized moment [11] from the rest of the background [12] has remained elusive. A mean field explanation at the level of linear spin wave theory (LSWT) does not yield meaningful results [13]; the usual Néel state is a not a good starting point, owing to the presence of coexisting locally disordered and ordered regions created by dilution. Therefore an attractive possibility for explaining this effect is the Schwinger boson mean field theory (SBMFT) for quantum antiferromagnets [14,15], which is capable of capturing a wide variety of phases.

The purpose of this paper is thus twofold. Our first aim is to demonstrate the utility of SBMFT in the context of dilution disorder. Going beyond limited functional forms for the mean field parameters, often used for clean systems, we instead numerically optimize all the parameters to minimize the energy, subject to them satisfying certain constraint equations. We find excellent qualitative agreement with respect to accurate many-body ground-state calculations carried out with density matrix renormalization group (DMRG) [16].

The second and main aim of the paper is to *interpret* the meaning of (1) the parameters corresponding to the lowest-energy solution and (2) the low-lying single-particle modes obtained from SBMFT. This framework explains the *fundamental* reason for the near decoupling of "dangling regions" in a diluted system. Our calculations have been carried out for Heisenberg antiferromagnets (HAF) on the square and Bethe lattices site-diluted to their percolation threshold (which corresponds to 40.72% and 50% dilution respectively). While the square lattice case has been extensively studied and is relevant experimentally [17], similar qualitative insights have been gained by studying the problem by eliminating loops (Bethe lattice) [4].

The dangling regions weakly interact with each other over the rest of the sites and form an effective unfrustrated low-energy system of their own that maintains long-range order in this system. We provide evidence for these assertions by studying the single-particle spectrum of SBMFT carefully and showing the existence of Goldstone modes. These modes are found to significantly differ from the corresponding LSWT counterparts; the latter is partially improved by the inclusion of quartic terms which are treated in a self-consistent Hartree Fock formalism. Finally, we connect our SBMFT results with many-body calculations and use the numerical spin-spin correlators from the theory to obtain a bound on the lowest energy scale within a single-mode approximation (SMA) formalism.

II. SCHWINGER BOSON MEAN FIELD THEORY (SBMFT) FORMALISM

SBMFT [14,15] has been widely successful in capturing a variety of ordered and disordered phases of Heisenberg

*Deceased.

Hamiltonians on regular lattices [18–21]. In particular, SBMFT has had good quantitative agreement with many-body numerical results for systems with long-range magnetic order [22] and in cases where true *physical* excitations of the HAF can be created at the mean field level using SBMFT parameters [23]. However, only a few studies exist where SBMFT or fermionic $\mathbb{SU}(N)$ theories have been applied to probe spatially nonuniform states [24–27]. Percolation clusters, with their nonuniform geometry, create a natural setting for studying spatially inhomogeneous mean field states.

Here we study the nearest-neighbor $S = 1/2$ HAF,

$$\mathcal{H} = \sum_{\langle ij \rangle} J_{ij} \mathbf{S}_i \cdot \mathbf{S}_j \tag{1}$$

with uniform couplings $J_{ij} = J$ on the square and coordination-3 Bethe lattices diluted to the percolation threshold. For this Hamiltonian, the $\mathbb{SU}(2)$ spin operators are mapped to two *flavors* of Schwinger bosons, using the relations

$$\mathbf{S}_i^+ = b_{i1}^\dagger b_{i2}, \quad \mathbf{S}_i^- = (\mathbf{S}_i^+)^\dagger, \quad 2\mathbf{S}_i^z = (b_{i1}^\dagger b_{i1} - b_{i2}^\dagger b_{i2}), \tag{2}$$

where $b_{im}^\dagger$ (b_{im}) is the creation (annihilation) operator for a boson of flavor m ($m = 1,2$) at site i. Once this substitution is performed, the resulting Hamiltonian is quartic in the bosonic operators and is decoupled by extending the number of flavors from two to N in either the $\mathbb{SU}(N)$ [14] or Sp($2N$) [15] approach.

We outline the former approach [28], which is valid for bipartite lattices. Within this formalism, the mean field Hamiltonians for each boson flavor m are identical and given by

$$\mathcal{H}_{MF}^m = \boldsymbol{\beta}^\dagger \begin{pmatrix} \Lambda & \mathbf{Q} \\ \mathbf{Q}^\dagger & \Lambda \end{pmatrix} \boldsymbol{\beta} + \frac{1}{J} \sum_{i<j} |Q_{ij}|^2 - \left(S + \frac{1}{2}\right) \sum_i \lambda_i, \tag{3}$$

where S is the spin length and $\boldsymbol{\beta}$ is a vector given by $\boldsymbol{\beta}^T = (b_{1m}, \ldots, b_{N_s m}, b_{i1}^\dagger, \ldots, b_{N_s m}^\dagger)$, with N_s being the number of sites on the lattice.

The matrix $\boldsymbol{\Lambda}$ is diagonal in the site basis with entries given by Lagrange multipliers $\lambda_i \delta_{ij}/2$ which enforce the "number constraint" on the bosons,

$$\sum_m \langle b_{im}^\dagger b_{im} \rangle = NS, \tag{4}$$

which is only satisfied on *average*. This constraint maps the Hilbert space of the bosons to that of spins. The expectation $\langle \cdots \rangle$ for evaluating the boson number expectation is taken in the Schwinger boson mean field state.

The matrix $\mathbf{Q}$ has entries that are all off-diagonal and are in general complex valued. On loop-less lattices like the diluted Bethe lattice, the *bond variables* Q_{ij} can be chosen to be real as there are no nontrivial loop fluxes [20,26] arising from the phases of the bond variables. Physically, these parameters denote the strength of the pairing amplitude of bosons; in the spin language they denote the strength to form a spin singlet between sites i and j. The optimal Q_{ij} values in the mean field state satisfy $Q_{ij} = \langle Q_{ij} \rangle = (J/N) \sum_{\langle i,j \rangle, m} \langle b_{im} b_{jm} \rangle$, where the expectation is again taken in the Schwinger boson mean field state and summed over the two flavors $m = 1,2$ (for number of flavors $N = 2$).

In general, the theory allows for extended-neighbor mean field parameters (i.e., any pair i, j), but in this paper we retain nonzero $\{Q_{ij}\}$ corresponding only to nearest neighbors. In practice, this restriction is generally found to give solutions that qualitatively match results from many-body calculations.

The set of mean field parameters $\{\lambda_i, Q_{ij}\}$, collectively called an ansatz, completely specifies the solutions of SBMFT. They are determined variationally by minimizing the mean field energy $\langle \mathcal{H}_{MF}^m \rangle = e_{MF}^m$, subject to constraints. e_{MF}^m is obtained by first solving the eigenvalue problem [29],

$$\begin{pmatrix} \boldsymbol{\Lambda} & \mathbf{Q} \\ -\mathbf{Q}^\dagger & -\boldsymbol{\Lambda} \end{pmatrix} \begin{pmatrix} u_n \\ v_n \end{pmatrix} = \omega_n \begin{pmatrix} u_n \\ v_n \end{pmatrix}, \tag{5}$$

which gives the single-particle Bogoliubov modes labeled n with frequencies $\{\omega_n\}$. This diagonalization gives $2N_s$ frequencies which occur as N_s $\pm |\omega_n|$ pairs. It is only the positive set of frequencies that is relevant for the quasiparticle spectrum. The wave functions corresponding to these frequencies are denoted as $\{u_{\rm in}, v_{\rm in}\}$. A linear combination of the modes $u_{\rm in}, v_{\rm in}$ is taken to define a length N_s mode on the lattice,

$$\psi_{\rm in}^\pm = u_{\rm in} \pm v_{\rm in}, \tag{6}$$

where $\psi_{\rm in}^\pm$ are eigenvectors of an $N_s \times N_s$ matrix with eigenfrequencies $\{\omega_n^2\}$; more details of this matrix have been discussed elsewhere [30]. For the lowest frequency SBMFT modes, we found $u_{\rm in}$ ($v_{\rm in}$) to be zero (nonzero) on one sublattice and nonzero (zero) on the other. For such modes, we fix the choice of gauge in the definition of $\{Q_{ij}\}$ by defining all values to be positive or negative, so that the wave function has a staggered sign pattern. The resultant mode, which we refer to as $\psi_{\rm in}$, is then used to compute all further operator expectations. This choice of gauge is completely equivalent to a choice of a uniform sign pattern and does not change the expectations of any physical observables.

The zero-point quantum energies $\{\hbar\omega_n/2\}$ are summed to get e_{MF}^m (the mean field energy per flavor),

$$e_{MF} = \sum_{n=1}^{n=N_s} \frac{1}{2} \omega_n + e_{\rm classical}, \tag{7}$$

where equivalence between flavors allows for the dropping of the flavor index m and $e_{\rm classical} = (1/J) \sum_{\langle ij \rangle} Q_{ij}^2 - (S + \frac{1}{2}) \sum_{i=1}^{i=N_s} \lambda_i$. Connection with the *physical* Heisenberg spins is made for $N = 2$, and the energy for this special case is given by $E_{Heis} = 2e_{MF} + \sum_{ij} J_{ij} S^2$.

The optimal ansatz $\{\tilde{\lambda}_i, \tilde{Q}_{ij}\}$ satisfies the "number constraint" and the "bond constraint": $\tilde{Q}_{ij} = \langle \tilde{Q}_{ij} \rangle$, which are implemented by introducing cost functions,

$$C_\lambda \equiv \sum_i (\langle b_i^\dagger b_i \rangle - S)^2, \quad C_Q \equiv \sum_{\langle ij \rangle} (Q_{ij} - \langle Q_{ij} \rangle)^2, \tag{8}$$

which are made as small as possible. The constrained optimization of the mean field variables $\{\lambda_i, Q_{ij}\}$ is thus transformed to a minimization problem through the cost functions C_Q, C_λ, which we perform efficiently using the Levenberg-Marquardt algorithm [26,31]. Typically, we found that these costs for the

solutions reported are in the range of 10^{-19}–10^{-16} (note the square root is above machine precision).

The geometry of the diluted Bethe lattice allows for a simplification in the initial choice of the bond amplitudes $\{Q_{ij}\}$, thereby improving the speed and scalability (to larger system sizes) of the optimization algorithm. Specifically, the lack of loops on the diluted Bethe lattice implies the absence of fluxes, and this allows us to choose all initial $\{Q_{ij}\}$ to be real. The computational complexity of the algorithm on the Bethe lattice scales as $\sim\tau_Q\tau_\lambda N_s^3$, where τ_λ (τ_Q) is the number of optimization steps to minimize C_Q (C_λ) and N_s^3 is the complexity of diagonalizing the mean field Hamiltonian (3) once. However, for the diluted square lattice the bond amplitudes Q_{ij}, in general, can be complex valued. This leads to U(1) fluxes Φ through even-length loops on the lattice, defined in the following gauge invariant manner:

$$\Phi = Q_{ij}(-Q^*_{jk})Q_{k\ell}\cdots(-Q^*_{pi}), \tag{9}$$

where Q^*_{jk} refers to the complex conjugate of Q_{jk}. The smallest nontrivial even-length loop on the square lattice is a square plaquette.

The optimization algorithm is started by allowing all initial Q_{ij} to be complex, and both the real and imaginary parts of the bond amplitudes are updated at every step of the self-consistent cycle to minimize C_Q (8). Since the number of effective constraints entering C_Q double (real and imaginary parts for each bond), the computational cost of optimization is roughly twice that of the diluted Bethe lattices [32]. The optimal mean field ansatz $\{\tilde{\lambda}_i, \tilde{Q}_{ij}\}$ on diluted square lattices always expels fluxes such that the optimal state has zero flux through all even length loops on the lattice. This was verified by starting the optimizer with several initial distributions of bond amplitudes which threaded nonzero fluxes through loops on the lattice. As the optimization proceeded, the flux pattern of the state was tracked, and in all cases we found the ground state to be a zero-flux state.

Finally, we remark that we studied specific instances of both kinds of clusters for generating insights and confirming our assertions. However, all analyses involving disorder averaging were studied only for the Bethe lattice case.

III. SBMFT PARAMETERS AND SINGLE-PARTICLE MODES

The interplay between the various contributions to e_{MF} in Eq. (7) can be understood heuristically. For a uniform one-dimensional chain of length L [33] the frequency $\{\omega_n\}$ for $\{\lambda_i = \lambda, Q_{ij} = Q\}$, momentum k_n, and coordination z are given by $\omega_n = \sqrt{\lambda^2 - [zQ\cos(k_n)]^2}$ [14]. For $zQ/\lambda < 1$ we have $\omega_n \sim \lambda - cQ^2/\lambda$ (c absorbs the momentum dependence), implying that ω_n is minimized when Q^2 is maximized and λ is minimized. On the other hand, the second and third terms, i.e., "classical terms" in (3), favor the opposite, i.e., low Q^2 and high λ. This competition between contributions to the energy can be complicated, especially in the case of a disordered system, and thus demands a numerical optimization.

Our results for the optimal ansatz for representative Bethe and square lattices at percolation are shown in Figs. 1(a) and 1(c), respectively. In both figures, the thickness of the bonds is proportional to $|\tilde{Q}_{ij}| - \min\{|\tilde{Q}_{ij}|\}$, and the radius of the disk on every site is proportional to λ_i^* at that site.

The distribution of optimal $\{|\tilde{Q}_{ij}|\}$ in Figs. 1(a) and 1(c) is a prescription for identifying pairs of spins with the strongest spin-spin correlations. Since the nearest-neighbor spin correlations are proportional to the pairing amplitudes $\langle \mathbf{S}_i \cdot \mathbf{S}_j \rangle = 3\tilde{Q}_{ij}^2/2$, the mean field ground state exhibits strong dimerization (pairing of nearest-neighbor spins into singlets) as was predicted in DMRG calculations [4]. Dimerizing nearest-neighbor spins for the strongest $|\tilde{Q}_{ij}|$ bonds pairs up all but two spins on each of the clusters in Figs. 1(a) and 1(c).

The distribution of $\{\tilde{\lambda}_i\}$ is proportional to the local coordination of the site; singly coordinated sites have small $\tilde{\lambda}_i \sim 0.5$, and triply coordinated sites have large $\tilde{\lambda}_i \sim 2.5$. The $\{\tilde{\lambda}_i\}$ field acts like an on-site disordered potential for the bosons. This can be observed in the low-frequency wave functions ψ_{in} given by Eq. (6), which avoid sites with high values of the potential, as shown in Figs. 1(b) and 1(d). The radii of the disks in Figs. 1(b) and 1(d) are proportional to wave function amplitudes, and the sign is encoded in the red (positive) and blue (negative) colors. Bosons have the highest amplitude of being on sites with the lowest potentials.

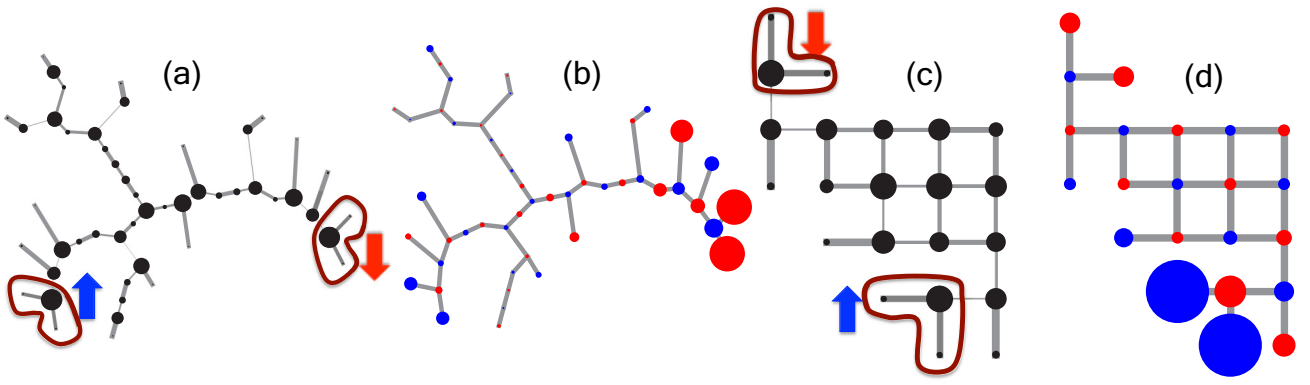

FIG. 1. (Color online) (a) and (c) The optimized SBMFT parameters λ_i, proportional to radius of circles on sites, and $|\tilde{Q}_{ij}| - \min\{|\tilde{Q}_{ij}|\}$ for nearest-neighbor bonds, proportional to the thickness of the bonds, on a diluted Bethe and square lattices, respectively. (b) and (d) The lowest single-particle eigenmode ψ^+_{i0}, whose amplitude is proportional to the radius of the circles and sign is denoted by the color. For more details about the interpretation of the parameters and eigenmodes refer to the text.

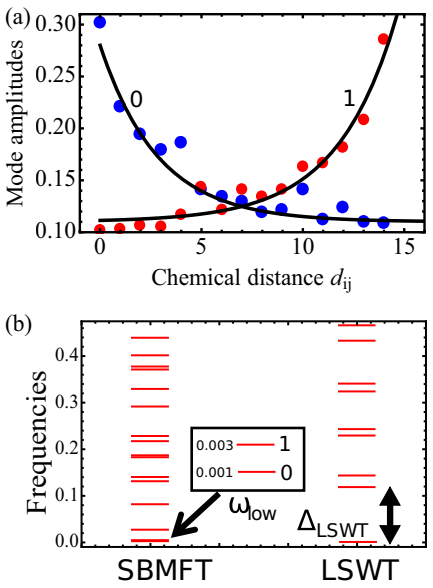

FIG. 2. (Color online) (a) Mode amplitudes ψ_{in} for the two lowest-frequency single-particle modes $n = 0, 1$ for the Bethe lattice percolation cluster shown in Figs. 1(a) and 1(b). Each mode (blue or red points) is plotted as a function of separation from the dangling spin at the fork tips. The fitted exponential decay is shown by solid black lines. (b) Single-particle frequencies for the same cluster obtained within SBMFT and LSWT. The two *anomalously* low Goldstone frequencies are indicated by an arrow and labeled as $\omega_{\ell ow}$; their numerical values and mode numbers n are indicated in the inset. The lowest nonuniform spin wave frequency is indicated by Δ_{LSWT}.

The two lowest-frequency modes are each localized on "fork" regions of three sites [encircled in Figs. 1(a) and 1(c)] and decay exponentially into the cluster [Fig. 2(a)]. An exponential fit to the mode on the Bethe lattice gives a decay constant $\xi_{\ell oc}$ of about 3 lattice spacings. These localized wave functions are the SBMFT characterization of *emergent* dangling spins on the cluster and are completely analogous to similar mode profiles obtained in many-body calculations [4].

The association of dangling spins with exponentially localized modes is a generic feature of both Bethe and square lattice percolation clusters. We check this by using a geometrical algorithm [4] by isolating 50-site Bethe lattice clusters with two dangling forks and fitting exponentially decaying functions of the distance away from the fork tip to the two lowest-energy modes. The fits give disorder-averaged $\langle \xi_{\ell oc} \rangle_{\text{dis.}} \sim 3$ lattice spacings in good agreement with the decay length of effective interactions [4]. This agreement is also indicative of the fact that the strength of effective interactions is proportional to the spatial overlap of the two modes.

IV. NONUNIFORM GOLDSTONE MODES IN SBMFT

A. Number of modes and effects of intermode interactions

The correspondence between dangling spins and localized bosonic modes in Fig. 1 strongly suggests that each dangling spin leaves its own characteristic signature in the SBMFT single-particle spectrum: a low frequency and an associated localized mode. This implies that the count of low-energy frequencies in the single-particle spectrum must match the number of dangling spins on the cluster.

We carry out a systematic check of this assertion by taking an ensemble of clusters and deploying techniques developed previously [4] to filter out the low-energy single-particle spectrum $\{\omega_{\ell ow}\}$ for each cluster in the ensemble. The count of frequencies in $\{\omega_{\ell ow}\}$ is then tallied against the number of dangling spins on a cluster, determined using a geometrical algorithm [4]. The situation is complicated by the fact that these emergent spins are not totally decoupled; their interactions push certain single-particle frequencies to higher energies and some to much lower energies. Thus the counts are found to agree in ∼92% of cases. Part of this discrepancy also arises from spatially extended dangling regions, which effectively leads to enhanced interactions with other localized dangling spins.

Among this set of low frequencies $\{\omega_{\ell ow}\}$, we found that two of them were driven to *anomalously* low values. These two *anomalously* low frequencies are shown for the Bethe percolation cluster from Fig. 1 in Fig. 2(b). The SU(2) invariance of the SBMFT formalism, along with the fact that these calculations are done on a finite cluster, prevents these two frequencies from becoming exactly zero. However, in the thermodynamic limit or in the presence of a small magnetic field, these *anomalously* low frequencies will be the first to become zero, causing bosons to condense into this mode. This signals long-range order within SBMFT and allows identification of the two *anomalously* low frequencies as the finite size manifestation of Goldstone modes on the cluster.

B. Failure of linear spin wave theory

The Goldstone modes, as seen in Figs. 1(b) and 1(d), have nonuniform amplitudes, significantly different from the zero-energy uniform Goldstone modes seen in LSWT [30]. These results suggest that SBMFT, in a single unified framework, characterizes emergent dangling degrees of freedom by associating localized modes with each of them, along with correctly predicting a background of long-range Néel order [12]. The maximal amplitude of Goldstone modes on the dangling sites provides direct evidence for the crucial role of dangling spins in stabilizing long-range order on the cluster. Based on these insights, we develop a better understanding for why LSWT fails to qualitatively capture the nonuniformities associated with the Goldstone modes.

The crucial difference between the LSWT and SBMFT approaches is that the former breaks spin rotational symmetry, leading to the inability to capture the *anomalous* lowering of frequencies associated with emergent SU(2) invariant dangling spin excitations. A comparison between LSWT and SBMFT single-particle frequencies in Fig. 2(b) for the Bethe percolation cluster in Figs. 1(a) and 1(b) shows that the lowest LSWT frequency is much higher than the corresponding frequency within SBMFT (LSWT has two exactly zero frequency uniform amplitude modes by construction). We generalize this observation by taking an ensemble of 50-site Bethe percolation clusters and plotting the disorder-averaged density of states (DOS) $\langle \rho(\log[\omega/J]) \rangle_{\text{dis.}}$, $\langle \rho(\log[\omega_{LSWT}/J]) \rangle_{\text{dis.}}$ within SBMFT and LSWT, respectively. The DOS on a logarithmic scale, calculated within LSWT and SBMFT, is shown in

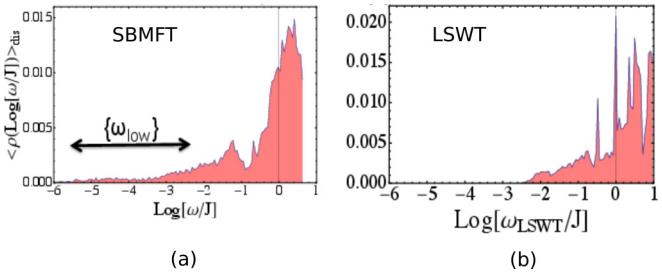

FIG. 3. (Color online) Disorder-averaged single-particle density of states within (a) SBMFT and (b) LSWT frameworks. An ensemble of 400 Bethe lattice percolation clusters, each consisting of 50 sites, was considered. The histograms were generated by grouping frequencies in bins of size $0.01J$. The SBMFT calculations show a set of low-lying frequencies missing in the LSWT spectrum, which have been labeled as $\omega_{\ell ow}$.

Figs. 3(a) and 3(b), respectively. The presence of an additional low-energy scale is seen in the SBMFT DOS and is indicated by a probability distribution with a long tail labeled $\omega_{\ell ow}$.

This discussion motivates us to look closely at the connection between the two approaches. We note that the LSWT Hamiltonian maps *exactly* to a SBMFT Hamiltonian with *fixed* λ_i and Q_{ij}. In LSWT, λ_i equals the coordination of the site, but in SBMFT this variable is a degree of freedom that is optimized. Since the optimal SBMFT solution is found to deviate significantly from the corresponding LSWT prediction, we conclude that it is this variational freedom that allows the lowest-energy modes to have nonuniform amplitudes, with largest weights in dangling regions.

Evidence for the *tendency* to form localized modes can be seen by including higher-order terms in the spin wave expansion; for the purpose of this paper we have retained the order $1/S$ terms. A Hartree-Fock (HF) decoupling of the quartic terms is applied, and the resultant mean field equations are solved self-consistently. Every iteration of our calculation cycle lowered the energy and showed gradual localization of the lowest modes, but we were unable to converge our solutions. This is not a problem with our implementation; instead it is evidence of growing spin fluctuations which eventually violate the assumptions of the Holstein-Primakoff expansion. The general inadequacy of LSWT and partial improvement with HF compared to SBMFT are confirmed with our results for certain spin-spin correlators shown in Fig. 4, where the three methods are compared to the corresponding near-exact DMRG values. (For a detailed exposition of the calculation of transverse correlations in spin wave theory, we refer the reader to Ref. [34].)

V. SBMFT CORRELATORS AND EFFECTIVE INTERACTIONS BETWEEN EMERGENT SPINS

A. Comparison of SBMFT and exact calculations

Through our computations for percolation clusters, we have shown that SBMFT can capture the correct qualitative physics of disordered systems. The next step is to assess the accuracy of the method with respect to many-body calculations, as a means of establishing the legitimacy of our conclusions. A useful product of such comparisons is a better evaluation of

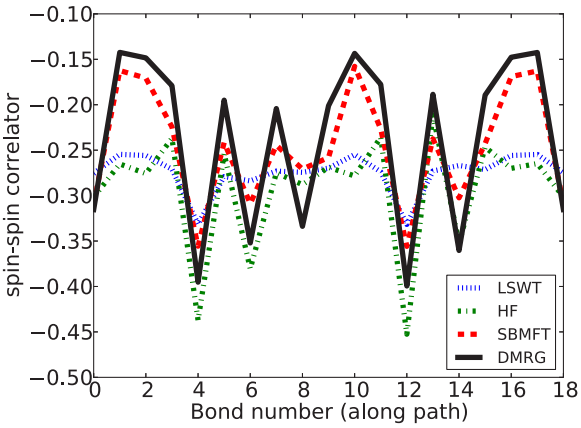

FIG. 4. (Color online) Nearest-neighbor in-plane spin-spin correlations, defined to be $\langle S_i^x S_j^x + S_i^y S_j^y \rangle$, for bonds taken along the path shown in Fig. 5(a), from various methods: linear spin wave theory (LSWT), Hartree-Fock (HF), Schwinger boson mean field theory (SBMFT), and the density matrix renormalization group (DMRG). The HF results are used from the iteration before the convergence of the self-consistency cycle failed. LSWT does not capture the variations in the values of the correlation functions, while going to order $1/S$ (S is the spin length) using HF shows tendency to capture the behavior of SBMFT and DMRG.

SBMFT as a computational tool in situations where performing accurate many-body calculations may be difficult.

In Figs. 5(a) and 5(b), for diluted Bethe and square lattices, respectively, we compare the DMRG and SBMFT spin-spin correlators for a reference site at the tip of the cluster and the other sites along a particular path. While we observe great qualitative agreement, quantitatively, our SBMFT calculation predicts slightly exaggerated oscillations at long distances.

A metric for a quantitative comparison of SBMFT versus DMRG is the ground-state energy per site obtained within SBMFT by summing over nearest-neighbor spin-spin correlations, defined as

$$e_{gs}^{SBMFT} = \frac{J}{N_s} \sum_{\langle i,j \rangle} \langle \mathbf{S}_i \cdot \mathbf{S}_j \rangle, \tag{10}$$

where the expectation $\langle \cdots \rangle$ is taken in the SBMFT ground state. The accuracy of the nearest-neighbor spin-spin correlations found within SBMFT as seen in Figs. 5(a) and 5(b) ensures that the maximum error in e_{gs}^{SBMFT} compared to the true ground-state energy from DMRG, for an ensemble of 400 clusters of 50-site clusters, is about 1%. A comparison of these estimates for our ensemble of clusters is shown in Fig. 5(c). We also note that e_{gs}^{SBMFT} serves as a better approximation of the ground-state energy of this model compared to the mean field energy e_{MF}. However, it is important to clarify that e_{gs}^{SBMFT}, just like e_{MF}, is nonvariational. The mean field state, which is used to compute both these energies, satisfies the boson number constraint (4) only on average.

B. Energy scale of effective interactions

SBMFT is primarily a tool to study singlet ground states, with no direct way to extract excited-state information. Here we use the ground-state SBMFT correlators to estimate the

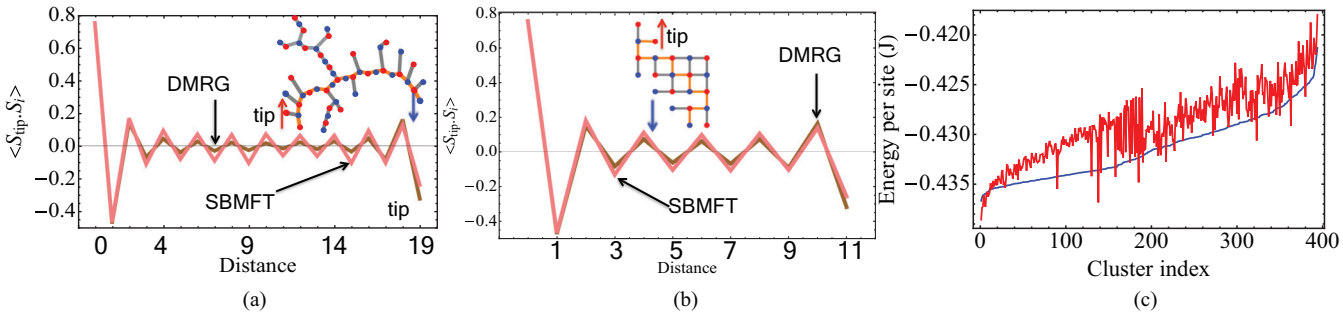

FIG. 5. (Color online) (a) Spin-spin correlations comparison between SBMFT and exact DMRG results for the Bethe cluster of Figs. 1(a) and 1(b), also shown in the inset. The correlations are between the tip spin labeled "tip" and all spins along the path shown in orange on the cluster. (b) Comparison of correlations similar to that in (a) for the square lattice cluster in Figs. 1(c) and 1(d). (c) Comparison between ground-state energies (sorted by value) from SBMFT (red) e_{gs}^{SBMFT} (10) and DMRG (blue) for an ensemble of 400 size 50 clusters. The SBMFT energy is obtained by summing over nearest-neighbor spin correlations.

singlet-triplet gap and hence the couplings between two weakly interacting emergent spins. This estimation is done within the single-mode approximation (SMA) formalism [35], which we briefly explain below. An alternate, but related, analysis maximizing the overlap of the SMA wave function with the true one (from DMRG) was also used previously by us [27].

In the SMA, the triplet excited state $|\Psi_{SMA}\rangle$ is created by taking a weighted superposition of single spin excitations of the ground-state SBMFT wave function, a singlet state ($S^{\rm tot}=0, S_z^{\rm tot}=0$),

$$|\Psi_{SMA}\rangle = \sum_{i=1}^{N_s} w_i S_i^+ |\Psi_{MF}\rangle, \tag{11}$$

where $\{w_i\}$ are variational weights determined by minimizing the SMA gap

$$\triangle_{SMA} = J\frac{\langle\Psi_{SMA}|\sum_{\langle ij\rangle}\mathbf{S}_i\cdot\mathbf{S}_j|\Psi_{SMA}\rangle}{\langle\Psi_{SMA}|\Psi_{SMA}\rangle} - E_0, \tag{12}$$

with E_0 being the ground-state energy.

For the Heisenberg model with uniform bond strengths, assuming a singlet ground state, an expression of the gap was derived previously [27],

$$\Delta_{SMA} = \frac{-J\sum_{\langle k,l\rangle}(w_k-w_l)^2 G_{kl}}{2\sum_{i,j} w_i\ w_j\ G_{ij}}, \tag{13}$$

where $\langle k,l\rangle$ are connected links, here the nearest neighbors, and $G_{ij}=\langle\Psi_{MF}|\mathbf{S}_i\cdot\mathbf{S}_j|\Psi_{MF}\rangle$. The notation in this expression implicitly assumes that these links are counted twice, i.e., once for k,l and the other for l,k, hence the factor of 2 in the denominator.

To obtain the optimal w_i, we define a quadratic cost function C_{SMA},

$$C_{SMA} \equiv \frac{-\sum_{\langle k,l\rangle}(w_k-w_l)^2 G_{kl}}{2} - \Lambda\left(\sum_{i,j=1}^{N_s} w_i w_j G_{ij} - 1\right), \tag{14}$$

where Λ is a Lagrange multiplier and is exactly equal to the SMA gap Δ_{SMA}. On differentiating C_{SMA} with respect to $\{w_i\}$ and setting the derivatives to zero, one gets a set of linear equations, which is compactly written as

$$\mathrm{Mw} = 2\Lambda\mathrm{Gw}, \tag{15}$$

where w is a compact notation for the vector $\{w_i\}$ and G denotes the matrix of spin-spin correlations with entries G_{ij}. M is a matrix with entries given by

$$M_{ii} = +2\sum_{\langle j\rangle} G_{ij}, \tag{16a}$$

$$M_{ij} = -2G_{ij} \quad \text{for } i,j \text{ connected}, \tag{16b}$$

$$M_{ij} = 0 \quad \text{otherwise}. \tag{16c}$$

where $\langle j\rangle$ refers to the set of sites j connected to site i. The generalized eigenproblem (15) is solved, and the minimum eigenvalue yields the SMA gap.

The optimized SMA gap provides an upper bound for the effective interactions between two dangling spins on opposite sublattices. Since we desire the distance dependence of effective couplings for extended objects, we define an "effective distance," analogous to that in Ref. [4], $\tilde{d}_{ij} = \sum_{n=1}^{n_d}\sum_{i,j}\psi_{\rm in}\psi_{jn}d_{ij}$, where $\psi_{\rm in}$ is the amplitude of the single-particle SBMFT mode n at site i and d_{ij} is the distance between sites (i,j). The sum over (i,j) runs over all pairs of sites that the two spins can delocalize over.

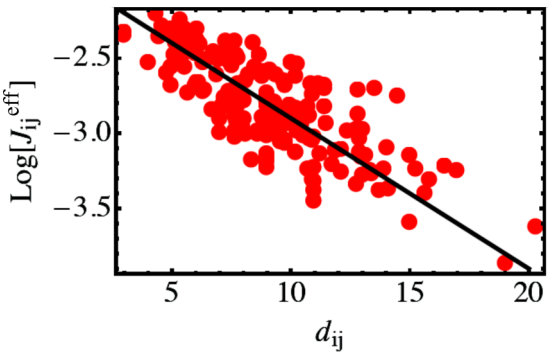

FIG. 6. (Color online) The decay of effective interactions $J_{ij}^{\rm eff}$ vs an effective distance $\tilde{d}_{ij}$ (see text). All data are for $N_s=50$ sized clusters.

We select percolation clusters from a randomly generated ensemble that have only two dangling spins on opposite sublattices. As shown in Fig. 6, we find their effective interactions to decay exponentially; a fit to $J_{ij}^{\rm eff} = J_0^* e^{-\tilde{d}_{ij}/\xi^*}$ gives $(J_0^*, \xi^*) = (0.15(2), 10.1(1))$. The decay length ξ^* is an upper bound on the decay constant $\xi \sim 5$ obtained from our previous DMRG study [4]. This slow decay of the interactions with distance is due to the inability of the SMA to describe very small gaps, a situation that occurs when the number of dangling spins is large. However, the qualitative prediction of exponentially decaying interactions is consistent with the occurrence of localized SBMFT modes associated with each dangling spin (region) as shown in Fig. 1.

VI. CONCLUSION

In summary, we have carried out Schwinger boson mean field theory (SBMFT) calculations for the case of nonuniform geometries, with specific emphasis on percolation clusters on the square and Bethe lattices. We show how the theory predicts the formation of emergent spin degrees of freedom arising due to local sublattice imbalance [4,5].

Our approach involved an interpretation of the mean field parameters, λ_i and Q_{ij}, which were the on-site potential and bond-pairing amplitude, respectively. We also showed that the low-lying single-particle wave functions have their largest amplitudes in regions associated with sublattice imbalance (i.e., the "dangling spins"). Thus, these modes provide a way of detecting emergent degrees of freedom on percolation clusters.

This interpretation is made firm based on the observation that the number of low-lying single-particle frequencies corresponds to the number of dangling spins on the cluster. The violations occur because the localized modes are not completely decoupled; interactions between them further split the single-particle energies. We generically found an additional lowering of the two lowest frequencies from this set; these were identified as the equivalent of (nonuniform) Goldstone modes. The fact that regions of sublattice imbalance are involved in these modes provides evidence for the link between the occurrence of emergent degrees of freedom and long-range order on the cluster, previously established numerically [12].

We explored how anharmonic effects in spin wave theory may explain the lowest modes seen in SBMFT; after all, the LSWT Hamiltonian maps *exactly* to a SBMFT Hamiltonian for large spin. In LSWT, the parameters λ_i are fixed by the coordination of the respective site i; on the other hand, in SBMFT they are variational parameters, which allows the lowest-energy modes to have nonuniform amplitudes with large weights in dangling regions. Evidence for the *tendency* to form localized modes for spin-1/2 is seen by going beyond LSWT, i.e., to order $1/S$ using self-consistent Hartree-Fock methods.

These observations also motivated a preliminary exploration of the role of spin length for the Heisenberg model on percolation clusters. Unlike the spin-1/2 case, we found our spin wave Hartree-Fock results to converge for the spin-1 case, which we take as evidence of the reduced role of spin fluctuations. Exact diagonalization calculations on small clusters also suggest that the picture of "emergent localized spins" may no longer apply for spin-1 as the distinction between the quasidegenerate states and the rest of the spectrum is not as clear as in the spin-1/2 case. This hints at the increased role of the bulk spins in the low-energy spectrum, expected for a spatially extended collective excitation.

Finally, we comment that SBMFT for disordered systems provides reasonable qualitative insights, complementing other highly accurate many-body calculations such as DMRG. We expect our implementation of SBMFT for nonuniform situations to perform equally well and scale favorably even in other dimensions. Based on results presented here and ongoing work, we believe the theory will be a useful tool in the treatment of frustrated lattices with disorder. In addition, in interesting cases like that of the Z_2 spin liquid on the kagome lattice, one can implement modifications to the theory that create excitations (visons), leading to numerical realizations of topological excitations [36].

ACKNOWLEDGMENTS

We thank A. Sandvik, D. Arovas, A. Auerbach, M. Lawler, R. Kaul, S. Pujari, and V. Chua for discussions. S.G. and C.L.H. acknowledge support from the National Science Foundation under Grant No. NSF-DMR 1005466. S.G. was also supported by a Cornell Graduate Fellowship. H.J.C. was supported by the SciDAC program of the U.S. Department of Energy (DOE) under Award No. DE-FG02-12ER46875. We acknowledge the Taub campus cluster at the University of Illinois at Urbana-Champaign and the CCMR facilities at Cornell University for computing resources.

[1] K. H. Hoglund and A. W. Sandvik, Phys. Rev. B **70**, 024406 (2004).
[2] A. J. Willans, J. T. Chalker, and R. Moessner, Phys. Rev. Lett. **104**, 237203 (2010); Phys. Rev. B **84**, 209901(E) (2011).
[3] A. Sen and R. Moessner, Phys. Rev. Lett. **114**, 247207 (2015).
[4] H. J. Changlani, S. Ghosh, S. Pujari, and C. L. Henley, Phys. Rev. Lett. **111**, 157201 (2013).
[5] L. Wang and A. W. Sandvik, Phys. Rev. Lett. **97**, 117204 (2006); Phys. Rev. B **81**, 054417 (2010).
[6] K. H. Hoglund, A. W. Sandvik, and S. Sachdev, Phys. Rev. Lett. **98**, 087203 (2007).
[7] K. H. Hoglund and A. W. Sandvik, Phys. Rev. Lett. **99**, 027205 (2007).
[8] A. Pal and D. A. Huse, Phys. Rev. B **82**, 174411 (2010).
[9] D. A. Huse, R. Nandkishore, and V. Oganesyan, Phys. Rev. B **90**, 174202 (2014).
[10] P. W. Anderson, Phys. Rev. **86**, 694 (1952); *Basic Notions of Condensed Matter Physics* (Benjamin, New York, 1984), pp. 44–46.
[11] C. L. Henley, and H. J. Changlani, J. Stat. Mech. (2014) P11002.
[12] A. W. Sandvik, Phys. Rev. B **66**, 024418 (2002).

[13] N. Bray-Ali, J. E. Moore, T. Senthil, and A. Vishwanath, Phys. Rev. B **73**, 064417 (2006).
[14] D. P. Arovas and A. Auerbach, Phys. Rev. B **38**, 316 (1988).
[15] N. Read and S. Sachdev, Phys. Rev. Lett. **62**, 1694 (1989).
[16] S. R. White, Phys. Rev. Lett. **69**, 2863 (1992).
[17] O. P. Vajk, P. K. Mang, M. Greven, P. M. Gehring, and J. W. Lynn, Science **295**, 1691 (2002).
[18] S. Sachdev, Phys. Rev. B **45**, 12377 (1992).
[19] L. Messio, B. Bernu, and C. Lhuillier, Phys. Rev. Lett. **108**, 207204 (2012).
[20] L. Messio, C. Lhuillier, and G. Misguich, Phys. Rev. B. **87**, 125127 (2013).
[21] C. H. Chung, J. B. Marston, and R. H. Mckenzie, J. Phys. Condens. Matter **13**, 5159 (2001).
[22] C. J. Gazza and H. A. Cecaato, J. Phys. Condens. Matter **5**, L135 (1993).
[23] T. Tay and O. I. Motrunich, Phys. Rev. B **84**, 193102 (2011).
[24] R. K. Kaul and M. Vojta, Phys. Rev. B **75**, 132407 (2007).
[25] M. Hermele and V. Gurarie, Phys. Rev. B **84**, 174441 (2011).
[26] G. Misguich, Phys. Rev. B **86**, 245132 (2012).
[27] H. J. Changlani, S. Ghosh, C. L. Henley, and A. M. Lauchli, Phys. Rev. B. **87**, 085107 (2013).
[28] We also carried out the Sp($2N$) formalism and verified the results to be consistent with the $\mathbb{SU}(N)$ approach outlined in text.
[29] J. H. P. Colpa, Physica A (Amsterdam, Neth.) **93**, 327 (1978).
[30] E. R. Mucciolo, A. H. Castro Neto, and C. Chamon, Phys. Rev. B **69**, 214424 (2004).
[31] M. I. A. Lourakis, LEVMAR, http://www.ics.forth.gr/~lourakis/levmar/.
[32] In practice, the U(1) gauge invariance of the flux equation (9) can be exploited to set a certain number of bond amplitudes to be purely real without changing the flux structure of the mean field state [26]. Hence, in practice, the computational cost of the optimization increases only by a factor between 1 and 2 compared to the Bethe lattice case.
[33] Similar functional dependencies of ω_n on λ and Q are found for small nonuniform geometries.
[34] U. Hizi and C. L. Henley, Phys. Rev. B **80**, 014407 (2009).
[35] R. P. Feynman, *Statistical Mechanics* (Benjamin, New York, 1972).
[36] M. J. Lawler, G. Y. Cho, and S. Ghosh (unpublished).